Biochemistry and Biophysics Reports 4 (2015) 134–140

Contents lists available at ScienceDirect

Biochemistry and Biophysics Reports

journal homepage: www.elsevier.com/locate/bbrep

Binding and structural studies of the complexes of type 1 ribosome inactivating protein from *Momordica balsamina* with cytosine, cytidine, and cytidine diphosphate

Shavait Yamini [1], S.N. Pandey [1], Punit Kaur, Sujata Sharma, T.P. Singh *

Department of Biophysics, All India institute of Medical Sciences, New Delhi, India

ARTICLE INFO

Article history:
Received 22 July 2015
Received in revised form
4 September 2015
Accepted 9 September 2015
Available online 11 September 2015

Keywords:
Ribosome inactivating protein
Crystal structure
Cytosine
Cytidine
Cytidine diphosphate

ABSTRACT

The type 1 ribosome inactivating protein from *Momordica balsamina* (*Mb*RIP1) has been shown to interact with purine bases, adenine and guanine of RNA/DNA. We report here the binding and structural studies of *Mb*RIP1 with a pyrimidine base, cytosine; cytosine containing nucleoside, cytidine; and cytosine containing nucleotide, cytidine diphosphate. All three compounds bound to *Mb*RIP1 at the active site with dissociation constants of 10^{-4} M–10^{-7} M. As reported earlier, in the structure of native *Mb*RIP1, there are 10 water molecules in the substrate binding site. Upon binding of cytosine to *Mb*RIP1, four water molecules were dislodged from the substrate binding site while five water molecules were dislodged when cytidine bound to *Mb*RIP1. Seven water molecules were dislocated when cytidine diphosphate bound to *Mb*RIP1. This showed that cytidine diphosphate occupied a larger space in the substrate binding site enhancing the buried surface area thus making it a relatively better inhibitor of *Mb*RIP1 as compared to cytosine and cytidine. The key residues involved in the recognition of cytosine, cytidine and cytidine diphosphate were Ile71, Glu85, Tyr111 and Arg163. The orientation of cytosine in the cleft is different from that of adenine or guanine indicating a notable difference in the modes of binding of purine and pyrimidine bases. Since adenine containing nucleosides/nucleotides are suitable substrates, the cytosine containing nucleosides/nucleotides may act as inhibitors.

1. Introduction

The ribosome inactivating proteins (RIPs) are N-glycosidases which are known to remove the specific purine residues from the sarcin/ricin (S/R) loop of the large rRNA [1,2]. This leads to the inhibition of protein synthesis in the cell [3]. The X-ray crystallographic studies have shown that RIPs bind specifically to adenine base [4]. A number of structures of type 1 RIPs from different sources in native forms [5–15] as well as of its several complexes with various ligands are already known [3,12,13]. The type 1 RIPs catalyze the removal of adenine residue from the sarcin/ricin loop (SRL) of rRNA in eukaryotic ribosomes [2,3]. These RIPs have also been shown to recognize the mRNA 5' cap structures with m^7GpppN motif where N is any base [12]. There are several reports about interactions of RIPs with purine bases of RNA such as adenine and guanine but no structural information is available on the mode of binding of pyrimidine bases such as cytosine and thymine. Therefore, it will be of interest to examine the modes of binding of pyrimidine bases to a type 1 RIP. We report here the binding studies of a type 1 RIP from *Momordica balsamina* (*Mb*RIP1) with three compounds, (i) cytosine (CYS), (ii) cytidine (CYT), and (iii) cytidine diphosphate (CDP). All three compounds bound to *Mb*RIP1 at the active site with dissociation constants of 10^{-4} M–10^{-7} M. The orientation of cytosine in the substrate binding cleft is found to be different from that of adenine and guanine in the complexes of *Mb*RIP1 with adenine and guanine [13].

2. Materials and methods

2.1. Isolation and purification

The purification of *Mb*RIP1 was carried out using the protocol reported earlier [13]. The samples of purified protein were concentrated using Amicon ultrafiltration device (Millipore Corporation, Bedford, USA) with a membrane having a molecular weight

* Correspondence to: Department of Biophysics, All India Institute of Medical Sciences, Ansari Nagar, New Delhi 110029, India. Fax: +91 11 2658 8663.
E-mail address: tpsingh.aiims@gmail.com (T.P. Singh).
[1] Contributed equally to this work.

http://dx.doi.org/10.1016/j.bbrep.2015.09.006

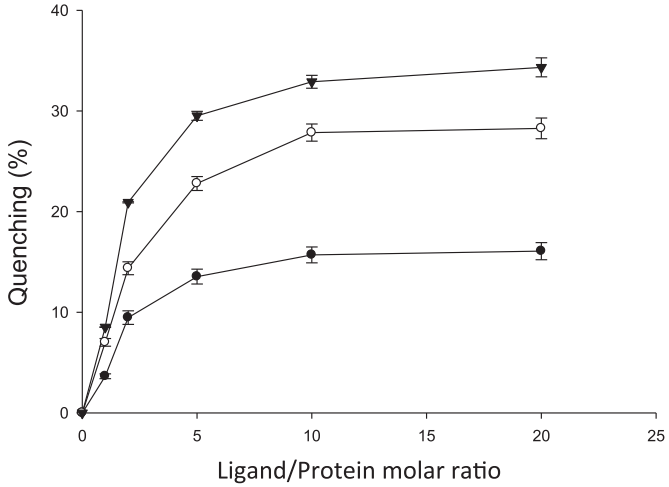

Fig. 1. Binding curves for cytosine (-•-), cytidine (-○-), and cytidine diphosphate (-▾-) showing the changes in fluorescence intensities ($\Delta F/F_o$) at 280 nm as the three compounds bound to *Mb*RIP1 with increasing molar concentrations of ligands. The errors on the experimental points have been indicated.

cut off of 3 kDa.

2.2. Binding studies using fluorescence

The binding studies of *Mb*RIP1 with compounds (i) CYS, (ii) CYT and (iii) CDP were carried out with spectrofluorometer FP -6200 (Shimadzu, Kyoto, Japan). 2.5 mg of protein was dissolved in 25 mM of sodium phosphate buffer at pH 6.8 at a concentration of 1×10^{-8} M. This solution was loaded in the 1 cm quartz cuvette. The stock solutions of CYS, CYT and CDP were also prepared in 25 mM sodium phosphate buffer pH 6.8 at concentrations of 1 mM. The concentration of all the three ligands were varied by adding increasing volumes of 1 μM, 2 μM, 5 μM, 10 μM, and 20 μM of CYS, CYT and CDP respectively from their stock solutions made at a concentration of 1 mM. The fluorescence experiments were conducted under the conditions of both entrance and exit slit widths at 5 nm and scanning speed of 240 nm/min. The fluorescence spectra of protein were recorded in the range of 300–400 nm at an excitation of 280 nm at 298 K (Fig. 1). All the observations were repeated six times for estimating the experimental errors. The spectral changes of the protein were recorded with different ligands at various concentrations.

Table1
Data collection and refinement statistics.

Parameter	CYS	CYT	CDP
PDB ID	4ZT8	5CSO	5CST
Space group	H3	H3	H3
Unit cell dimensions (Å)			
$a=b$	130.3	130.2	130.2
c	39.9	39.9	40.5
Number of molecules in unit cell	9	9	9
Resolution range (Å)	37.63–1.98	37.62–1.78	38.11–1.78
Total number of observed reflections	83496	149580	132103
Number of unique reflections	16671	22979	22958
Overall completeness of data (%)	99.9(99.8)	99.9(99.5)	99.8(96.9)
Overall R_{sym} [a] (%)	7.3(28.3)	5.0(27.2)	6.5(49.2)
Overall I/σ (I)	32.3(4.2)	51.2(4.8)	34.0(2.6)
R_{cryst} [b] (%)	17.9	18.5	15.5
R_{free} (%)	20.4	21.4	18.9
Protein atoms	1911	1911	1911
Ligand atoms (one molecule)	8 (CYS)	17(CYT)	25 (CDP)
Carbohydrate atoms (NAG)	14	14	14
Water molecules	220	246	245
R.m.s.d in bond lengths (Å)	0.01	0.01	0.02
R.m.s.d in bond angles (deg)	1.08	1.09	2.0
R.m.s.d in dihedral angles (deg)	13.1	12.4	12.3
Overall G factor	0.14	0.15	−0.02
Wilson B-factor (Å^2)	24.1	23.9	21.8
Mean B-factor for main chain atoms	28.7	28.2	25.7
Mean B-factor for side chain atoms and water oxygen atoms	32.5	33.4	33.1
Mean B-factor for all atoms	30.8	31.1	29.7
Residues in the most favored regions (%)	93.2	92.7	93.2
Residues in the additionally allowed regions (%)	6.4	6.8	6.4
Residues in the disallowed regions (%) (Leu 77 as part of type II′ β-turn)	0.5	0.5	0.5.0.2

The values in parentheses correspond to the values in the highest resolution shell.

[a] $R_{sym} = \sum_{hkl}\sum_i |I_i(hkl) - < I(hkl) >| / \sum_{hkl}\sum_i I_i(hkl)$ where I_i (hkl) is the intensity of the ith measurement of reflection hkl and $< I(hkl) >$ is the mean value of I_i (hkl) for all i measurements.

[b] $R_{cryst} = \sum_{hkl}|(F_{obs}) - (F_{cal})| / \sum_{hkl}|(F_{obs})|$ where F_{obs} is the observed structure factor amplitude and F_{cal} is the structure amplitude calculated from the model. R_{free} is the same as R_{cryst} except that it has been calculated with a 5% data that were excluded from the refinement calculations.

2.3. Binding studies using surface plasmon resonance spectroscopy

The surface plasmon resonance (SPR) measurements were carried out using Biacore-2000 (Pharmacia Biosensor AB, Uppsala, Sweden) at 25 °C in which a biosensor based system has been used for real time specific interaction analysis. The sensor chip CM5,

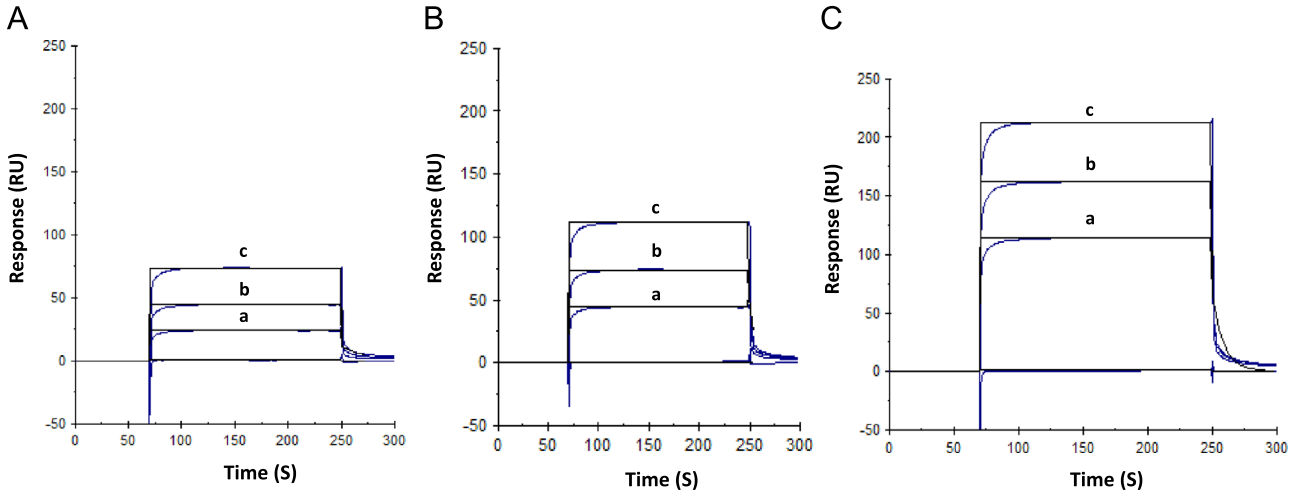

Fig. 2. Sensogram for the binding of analytes, (A) cytosine, (B) cytidine, and (C) cytidine diphosphate to *Mb*RIP1. The protein was immobilized on CM-5 chip and increasing concentrations (1 mM, 2 mM and 4 mM) of analytes were used in mobile phase corresponding to curves a, b and c respectively.

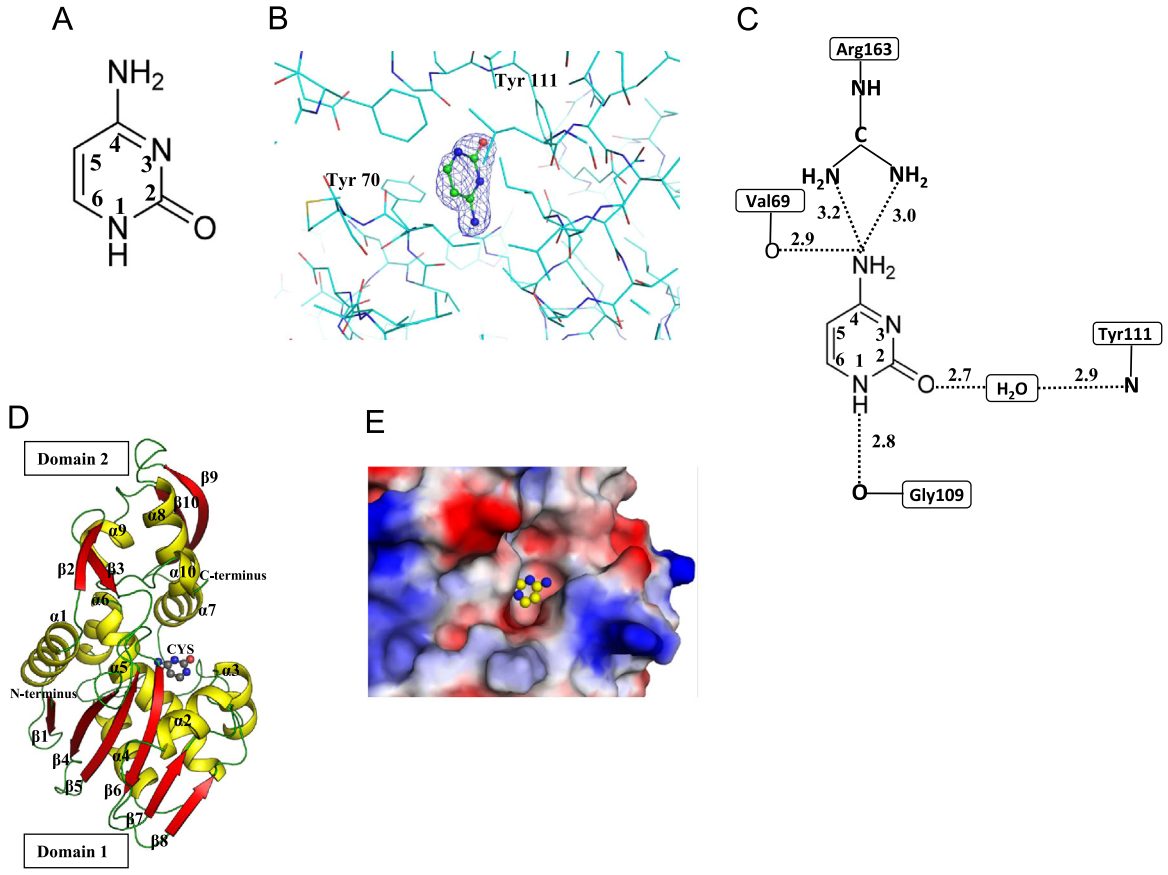

Fig. 3. (A) Schematic numbering of atoms in Cytosine, (B) the OMIT ($F_o - F_c$) (blue) electron density for cytosine at 3.0σ level, (C) hydrogen bonds between *Mb*RIP1 and cytosine are shown by dotted lines, (D) the ribbon diagram of *Mb*RIP1 with cytosine in the substrate binding cleft and (E) a grasp representation of the substrate binding cleft with cytosine in the cleft (ball and stick model). (For interpretation of the references to color in this figure legend, the reader is referred to the web version of this article.).

surfactant P20, the amine coupling kit containing N-hydroxyl succinimide (NHS), N-ethyl-N'-3(diethyl amino propyl) carbamide (EDC) and ethanolamine hydrochloride (Pharmacia Biosensor AB, Uppsala, Sweden) were used in the experiment. The immobilization of *Mb*RIP1 was performed at a flow rate of 10 µl/min using amine coupling kit. The dextran on the chip was equilibrated with running buffer and carboxy methylated matrix was activated with EDC/NHS mixture and 200 µl of *Mb*RIP1 (200 µg/ml) in 10 mM sodium acetate at pH 5.0, the unreacted groups were blocked by injecting ethanolamine (pH 8.5). The SPR signal for immobilized *Mb*RIP1 reached 14357.8 RUs. Three concentrations of analytes, 1.0 µM, 2.0 µM and 4.0 µM were passed over immobilized *Mb*RIP1 at a flow rate of 10 µl/min. The regeneration of protein surface from bound analyte was done using 10 mM glycine HCl at pH 3.0 (Fig. 2). The association (K_{on}) and dissociation (K_{off}) rate constants for the analytes bindings to *Mb*RIP1 were calculated and the values of dissociation constants (K_D) were determined by mass action relation $K_D = K_{off}/K_{on}$ using BIAevaluation 3.0 software provided by the manufacturer.

2.4. Crystallization

The freshly purified and lyophilized samples of *Mb*RIP1 were dissolved in 25 mM sodium phosphate buffer at pH 6.8 to a concentration of 20 mg/ml. CYS, CYT and CDP were also dissolved separately in the same buffer. The solutions of ligands were mixed separately with the protein solution in 1:1 (v/v) ratios and were incubated overnight at room temperature (~295 K). A solution containing 0.1 M sodium phosphate buffer pH 6.8 and 16% (v/v) polyethylene glycol 6000 (PEG-6000) was prepared as the reservoir buffer for the purpose of crystallization. It was mixed with each of the incubated solutions containing protein and ligand in 1:1 (v/v) ratio. The 6 µl drops of these solutions were prepared for the hanging drop vapor diffusion method at 298 K. After 10 days, cuboid shaped crystals from all the three sets of experiments were obtained.

2.5. X-ray intensity data collection and processing

Three X-ray intensity data sets were collected using one crystal each from the three samples containing complexes of *Mb*RIP1 with (i) CYS, (ii) CYT, and (iii) CDP. The crystals were mounted in nylon loops and frozen in liquid nitrogen stream at 100 K. For data collection MAR CCD scanner (MAR Research, Norderstedt, Germany) was used on the BM14 Beam line at the European Synchrotron Radiation Facility (ESRF, Grenoble, France). All the three data sets were indexed and processed using HKL-2000 package [16]. The summary of data collection statistics is given in Table 1.

2.6. Structure determination and refinement

The structures of the complexes of *Mb*RIP1 with CYS (Fig. 3A), CYT (Fig. 4A) and CDP (Fig. 5A) were determined with molecular replacement method [17] using coordinates of native protein as the model (PDB: 3S9Q) [13]. It gave the clear solutions. All the three structures were refined with REFMAC 5 [18] from the CCP4i Version 4.2 program package [19,20] for 25 cycles. After these cycles of refinement, the R_{cryst}/R_{free} factors for the three complexes reduced to values of 0.251/0.282, 0.241/0.281 and 0.261/0.283, respectively. The models were improved by manual model

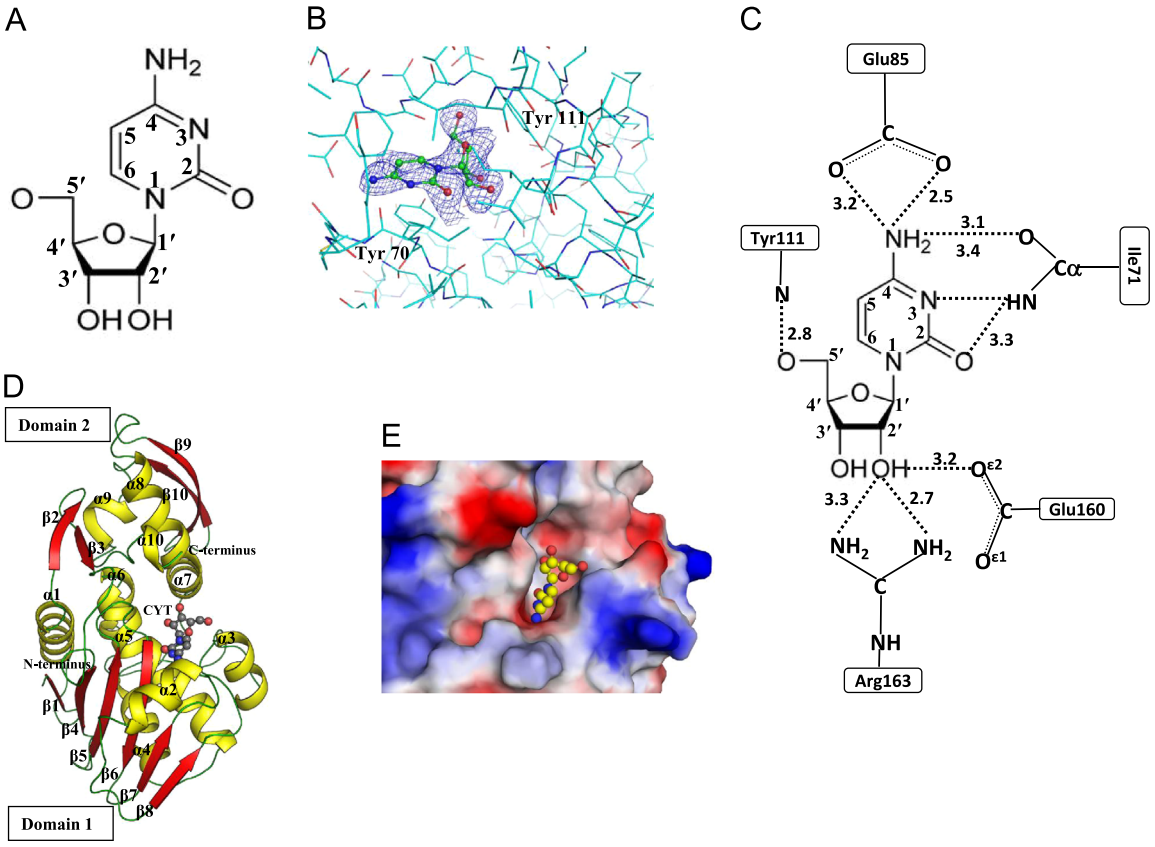

Fig. 4. (A) Schematic numbering of atoms in Cytidine, (B) the OMIT (F_o-F_c) (blue) electron density for cytidine at 2.5σ level, (C) hydrogen bonds between protein and cytidine atoms are shown with dotted lines, (D) the ribbon diagram of the protein with bound cytidine in the substrate binding cleft and (E) a grasp representation of the cleft with cytidine placed in the cleft. (For interpretation of the references to color in this figure legend, the reader is referred to the web version of this article.).

building with programs O [21] and Coot [22] on the graphics workstations. The difference (F_o-F_c) Fourier maps calculated at this stage revealed extra densities at the substrate binding site in *Mb*RIP1 into which molecules of CYS (Fig. 3B), CYT (Fig. 4B) and CDP (Fig. 5B) were fitted. These non-protein electron densities were observed at higher than 2.5σ. Out of these three compounds, the terminal phosphate of CDP is found in two conformations and is therefore modeled likewise as shown in Fig. 5B. The atoms of these compounds were included in the subsequent cycles of refinements. The same difference (F_o-F_c) Fourier maps were also used for locating the positions of water oxygen atoms. The positions of water oxygen atoms were picked up based on the isolated electron densities at more than 2.5σ and having spherical shapes with distances up to 3.5 Å from nitrogen and oxygen atoms of protein. This gave 220, 246, and 245 water oxygen atom positions for the complexes with (i) CYS, (ii) CYT, and (iii) CDP respectively. After including all these atoms in the further cycles, the refinement converged to value of 0.179/0.204, 0.185/0.214 and 0.155/0.189 for R_{cryst}/R_{free} factors for structures (i) to (iii) respectively. The final refinement statistics for all the three structures are included in Table 1. The refined atomic coordinates have been deposited in the Protein Data Bank (PDB) with accession codes of 4ZT8, 5CSO and 5CST, respectively.

3. Results

3.1. Analysis of binding studies using fluorescence spectroscopy

In order to determine the binding affinities of three ligands (i) CYS, (ii) CYT and (iii) CDP, the fluorescence properties of the binding site in *Mb*RIP1 were exploited. The intrinsic fluorescence of *Mb*RIP1 when excited at 280 nm is due to the presence of Tyr70 and Tyr111 in the substrate binding site. The fluorescence spectra were recorded in the presence of increasing amounts of ligands. The fluorescence intensities of *Mb*RIP1 decreased gradually when the concentrations of ligands were increased, although the positions of emission maxima as well the shapes of the peaks remained unaltered. This suggested that the binding of ligands to *Mb*RIP1 did not alter the environment in the vicinity of two aromatic residues. The observed fluorescence data were used for calculating the fluorescence quenching defined as $Q\%=(F_o-F)/F_o$, where F is the fluorescence intensity measured after the ligands were added to the solution of *Mb*RIP1 while F_o is the fluorescence intensity in the absence of ligands. Plots of graphs of Q (%) against the molar ratios of ligands to protein are shown in Fig. 1. The least-squares fits of the fluorescence intensity changes for the ligand/protein binding curves were obtained by Sigma Plot 8.0 [23]. The error bars on the experimental points were estimated from the average of values that were calculated using the binding equation described by Scatchard [24]. The approximate value of the dissociation constants (K_D) for the binding of (i) CYS, (ii) CYT and (iii) CDP were found to be 2.3×10^{-4} M, 5.0×10^{-6} M, and 2.8×10^{-7} M, respectively. These results indicated that all the three ligands bound to *Mb*RIP1 with significant affinities.

3.2. Determination of binding affinity using SPR

The molecular interactions between *Mb*RIP1 and its binding partners CYS, CYT and CDP, were studied in real time using SPR spectroscopy. The sensograms for the interactions with (i) CYS, (ii) CYT and (iii) CDP were shown in Fig. 2. The increase of resonance

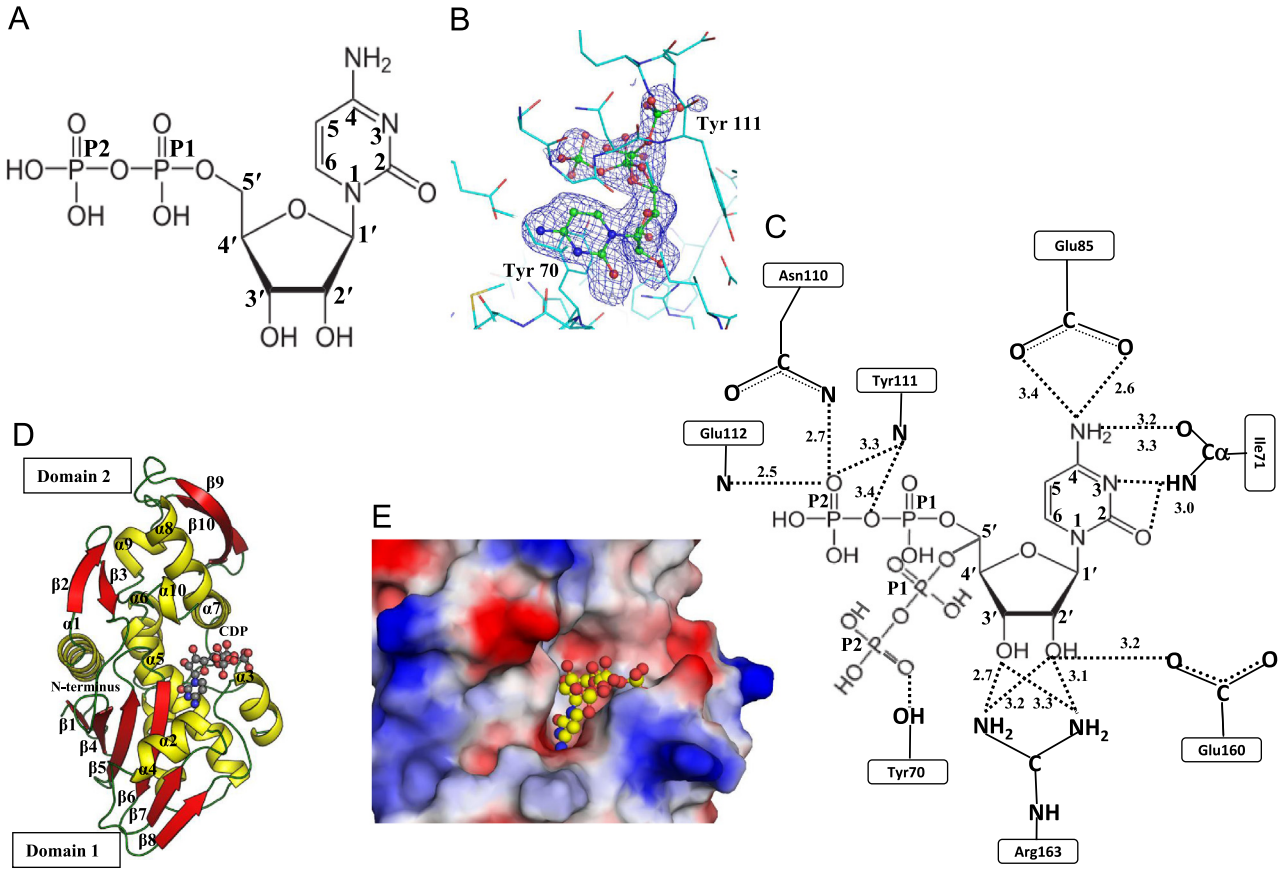

Fig. 5. (A) Schematic numbering of atoms in Cytidine diphosphate, (B) the OMIT ($F_o - F_c$) (blue) electron density for cytidine diphosphate at 2.5σ level, (C) hydrogen bonds between protein and cytidine diphosphate atoms are indicated by dotted lines, (D) the ribbon diagram for *Mb*RIP1 with cytidine diphosphate in the substrate binding site and (E) a grasp representation of the substrate binding cleft with cytidine diphosphate (in ball and stick representation) bound to it. (For interpretation of the references to color in this figure legend, the reader is referred to the web version of this article.).

units (RU) from the baseline represents the binding of ligands to the immobilized protein. The plateau line represents the steady state equilibrium phase of interactions between protein and the ligands whereas the decrease in RU from the plateau represents the dissociation phase. The values of dissociation constants (K_D) were calculated to be 4.1×10^{-5} M, 9.4×10^{-7} M and 1.1×10^{-7} M for the binding of CYS, CYT and CDP respectively.

3.3. X-ray structural studies

3.3.1. Structure of the complex of MbRIP1 with cytosine

The structure of the complex of *Mb*RIP1 with cytosine was determined at 1.98 Å resolution with 93.2% residues in the most favored regions of the Ramachandran map [25] as calculated using PROCHECK [26]. It may be mentioned here that the substrate binding site in the native structure contains ten water molecules which are interlinked through hydrogen bonds [16, PDB ID: 3S9Q]. Upon binding of cytosine, four out of ten water molecules were dislodged from the substrate binding site. The structure showed that cytosine formed five hydrogen bonds (Fig. 3C). The residues that formed direct hydrogen bonds with cytosine included Val69, Gly109 and Arg163 while Tyr111 interacted through a solvent water molecule. Cytosine also formed several van der Waals contacts with residues, Tyr70, Leu151 and Ile 155. The position of CYS in the substrate binding cleft is shown in Fig. 3D. It is clearly seen that cytosine is completely buried in the substrate binding pocket (Fig. 3E) with a buried surface area of 157 Å^2 as calculated using PISA server [21]. However, a significant space in the pocket was still unoccupied. The conformations as defined by torsion angles, χ^1 and χ^2 for the side chains of two important residues, Tyr70 andTyr111 of the substrate binding site were estimated to be -70° and 158°, and −81° and 140°, respectively.

3.3.2. Structure of the complex of MbRIP1 with cytidine

The structure of the complex of *Mb*RIP1 with cytidine was determined at 1.78 Å resolution. As calculated using PROCHECK [26], it showed that the 92.7% residues were present in the most favored regions of the Ramachandran map [25]. Upon the binding of cytidine to *Mb*RIP1, five out of ten water molecules were dislodged from the substrate binding site. The structure of the complex showed that the ligand is stabilized by nine hydrogen bonds (Fig. 4C). The residues that form hydrogen bonds include Ile71, Glu85, Tyr111, Glu160 and Arg163. Several van der Waals interactions have also been observed. The notable van der Waals contacts were formed with residues, Tyr70, Tyr111, Asn110 and Gly109. The orientation of cytidine in the substrate binding cleft can be seen in Fig. 4D. The cytidine molecule is fully buried in the cleft (Fig. 4E) with a buried surface area of 254.2 Å^2. In this case, the conformations of the side chains of Tyr70 and Tyr111 as defined by torsion angles, χ^1 and χ^2 were found to be −81° and −172°, and −83° and 141°, respectively.

3.3.3. Structure of the complex of MbRIP1 with cytidine diphosphate

The structure of the complex of *Mb*RIP1 with cytidine diphosphate (CDP) was determined at 1.78 Å resolution. As calculated using PROCHECK [26], the refined model has 93.2% of amino acid residues in the most favored regions of Ramachandran map [25]. Upon binding of CDP to *Mb*RIP1, seven out of ten water molecules were dislodged. The map indicates that the beta phosphate has two conformations. The structure of the complex showed that CDP

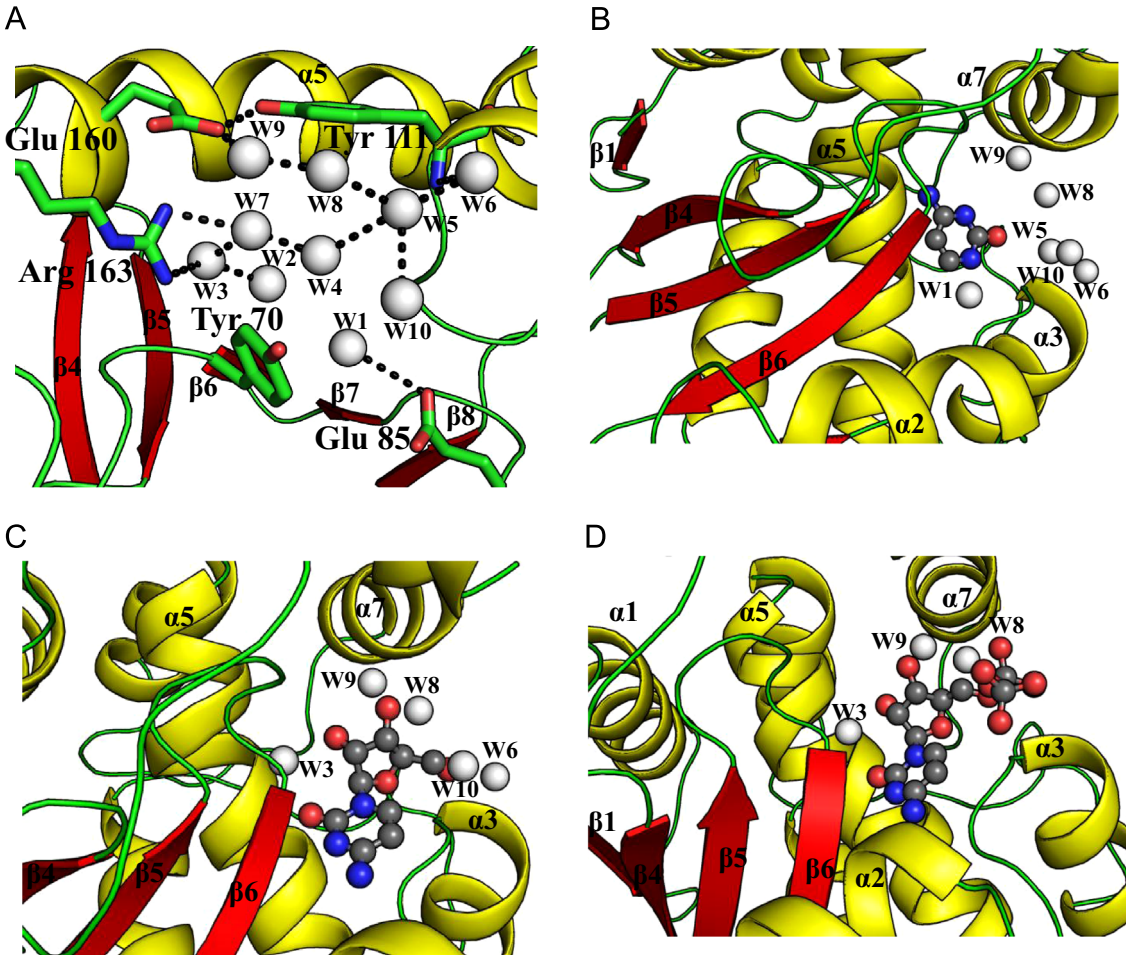

Fig. 6. (A) Ten water molecules, W1 (526), W2 (525), W3 (524), W4 (272), W5 (520), W6 (453), W7 (263), W8 (427), W9 (390), W10 (273) were observed in the substrate binding cleft of the native unliganded structure of *Mb*RIP1 (PDB ID: 3S9Q). The numbers in parentheses correspond to numbers in the PDB. (B) The binding of cytosine to *Mb*RIP1 replaced four water molecules, W2, W3, W4 and W7. (C) The binding of cytidine replaced five water molecules, W1, W2, W4, W5 and W7. (D) Upon binding of cytidine diphosphate seven water molecules, W1, W2, W4, W5, W6, W7 and W10 were removed from the substrate binding site.

formed at least 14 hydrogen bonds (Fig. 5C). It also formed several van der Waals contacts involving residues, Tyr70, Ile71, Tyr111, Asn110, Phe83, Gly109 and Glu112. The orientation of CDP in the substrate binding site can be seen from Fig. 5D. CDP is fitted well in the substrate binding cleft (Fig. 5E) with a buried surface area of 293.5 Å^2. In this case, the conformations of the side chains of Tyr70 and Tyr111 as defined by torsion angles, χ^1 and χ^2 were found to be $-77°$ and $-162°$, and $-77°$ and 135°, respectively.

4. Discussion

The rectangular substrate binding cleft in type 1 RIPs is situated between two domains. The amino acid residues that constitute the substrate binding cleft include Tyr70, Tyr111, Glu85, Ile155, Ala87, Asn110, Ile186, Glu160, Glu112, Asn68 and Arg163. In the native structure of *Mb*RIP1 (PDB ID: 3S9Q), ten water molecules, W1 to W10 were observed in the substrate binding cleft which were interconnected through hydrogen bonds (Fig. 6A). Upon binding to cytosine, four water molecules, W2, W3, W4 and W7 were dislodged from the cleft (Fig. 6B) while the binding of cytidine removed five water molecules, W1, W2, W4, W5 and W7 (Fig. 6C). When cytidine diphosphate bound to *Mb*RIP1, seven water molecules, W1, W2, W4, W5, W6, W7 and W10 were dislodged (Fig. 6D). This showed that three water molecules, W2, W4 and W7 were dislodged in all the structures indicating that it was a common subsite occupied by some parts of these compounds. The two water molecules, W8 and W9 remained present in all the structures indicating that these two locations were never occupied by these compounds. In the case of cytosine, two water molecules, W1 and W5 remained bound to protein while W3 was removed. In contrast, in both other structures, W1 and W5 were never observed while W3 was present. This indicated that the positioning of cytosine in the substrate binding cleft was slightly different from those occupied by other compounds. The molecule of cytidine diphosphate occupies the whole substrate binding site in *Mb*RIP1 and thus suggests that the optimum size for fitting the compound in the substrate binding site corresponds to cytidine diphosphate.

The type 1 RIPs are known to remove an adenine residue from the sarcin/ricin loop (SRL) of rRNA in eukaryotic ribosomes [2,3]. The structural studies have also shown that whenever adenine containing nucleosides and nucleotides were used for crystallization of the complexes with *Mb*RIP1, invariably, the complexes with adenine were obtained as these used to get hydrolyzed. It has also been shown that *Mb*RIP1 binds to mRNA 5'cap structures with m^{7}GpppN where N is any base [12]. The present structures showed that *Mb*RIP1 can also bind to cytosine and cytosine containing nucleoside and nucleotide. It is observed that cytosine, cytidine and CDP were fully buried in the cleft. It suggested that the optimum element for specificity in cytosine containing sequences of RNA structures is a nucleoside moiety. The number of interactions

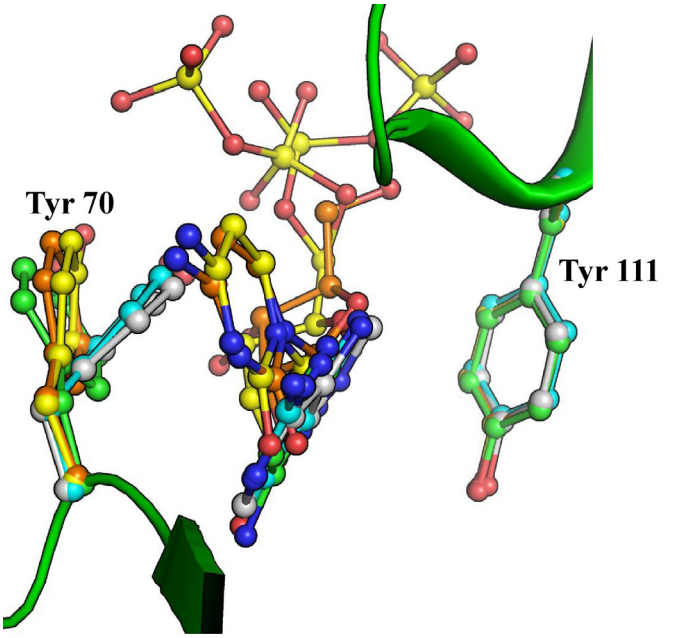

Fig. 7. Showing the orientations of the planes of aromatic rings of five ligands with respect to the planes of Tyr70 and Tyr111 in the complexes of *Mb*RIP1 with cytosine (green), cytidine (orange), cytidine diphosphate (yellow), adenine (grey) and guanine (cyan). (For interpretation of the references to color in this figure legend, the reader is referred to the web version of this article.).

observed with CDP were maximum indicating that it has the maximum binding affinity.

One of the main differences in the structure of protein upon binding of cytosine and cytosine containing compounds to *Mb*RIP1 as compared to those of adenine and guanine pertains to the conformation of the side chain of Tyr70. The values of the torsion angles, χ^1 and χ^2 for the side chain of Tyr70 in the complexes of cytidine and cytidine diphosphate were found centered at $-70°$ and $-165°$, respectively. The corresponding values in the complexes of *Mb*RIP1 with adenine and guanine were found to be centered at $-90°$ and $-75°$, respectively. The corresponding values in the unbound native structure were found to be $-66°$ and 165°, respectively. Clearly, in the three structural states, the conformations of the side chain of Tyr70 are very different (Fig. 7). It may be mentioned that the conformation of the side chain of Tyr111 remains the same in all the three states (Fig. 7). The orientation of the plane of the aromatic ring of cytosine with respect to that of the aromatic ring of Tyr70 was 130° while the corresponding angle in the complexes with adenine and guanine were centered at 165°. The plane of adenine ring in the cleft is oriented nearly parallel to the plane of the side chain of Tyr70 while that of cytosine is deviated considerably from parallel orientation. This difference is important for the catalytic activity of *Mb*RIP1. These differences may be responsible for the removal of adenine from the SRL of rRNA while cytosine cannot be removed because of different orientation in the cleft. However, it may act as an inhibitor of RIPs.

Acknowledgments

The authors thank Department of Biotechnology (DBT) of the Ministry of Science and Technology for sponsoring the beamline, BM14 at the ESRF, Grenoble, and France. TPS thanks the INSA, New Delhi for the grant under INSA Senior Scientist programme. SY thanks Indian Council of Medical Research, New Delhi and SNP thanks University Grants Commission, New Delhi.

Appendix A. Supplementary material

Supplementary data associated with this article can be found in the online version at http://dx.doi.org/10.1016/j.bbrep.2015.09.006.

References

[1] L. Barbieri, M.G. Battelli, F. Stirpe, Ribosome-inactivating proteins from plants, Biochim. Biophys. Acta 1154 (1993) 237–282.
[2] Y. Endo, K. Mitsui, M. Motizuki, K. Tsurugi, The mechanism of action of ricin and related toxic lectins on eukaryotic ribosomes. The site and the characteristics of the modification in 28S ribosomal RNA caused by the toxins, J. Biol. Chem. 262 (1987) 5908–5912.
[3] Y. Endo, K. Tsurugi, RNA N-glycosidase activity of ricin A-chain. Mechanism of action of the toxic lectin ricin on eukaryotic ribosomes, J. Biol. Chem. 262 (1987) 8128–8130.
[4] J. Ren, Y. Wang, Y. Dong, D.I. Stuart, The N-glycosidase mechanism of ribosome inactivating proteins implied by crystal structures of alpha-momorcharin, Structure 2 (1994) 7–16.
[5] W. Montfort, J.E. Villafranca, A.F. Monzingo, S.R. Ernst, B. Katzin, E. Rutenber, N. H. Xuong, R. Hamlin, J.D. Robertus, The three-dimensional structure of ricin at 2.8, J. Biol. Chem. 262 (1987) 5398–5403.
[6] J. Husain, I.J. Tickle, S.P. Wood, Crystal structure of momordin, a type I ribosome inactivating protein from the seeds of *Momordica charantia*, FEBS Lett. 342 (1994) 154–158.
[7] X. Hou, M. Chen, L. Chen, E.J. Meehan, J. Xie, M. Huang, X-ray sequence and crystal structure of luffaculin 1, a novel type 1 ribosome-inactivating protein, BMC Struct. Biol. 7 (2007) 29.
[8] Q.J. Ma, J.H. Li, H.G. Li, S. Wu, Y.C. Dong, Crystal structure of beta-luffin, a ribosomeinactivating protein, at 2.0 resolution, Acta Crystallogr. D: Biol. Crystallogr. 59 (2003) 1366–1370.
[9] S.L. Gawlak, M. Neubauer, H.E. Klei, C.Y. Chang, H.M. Einspahr, C.B. Siegall, Molecular, biological, and preliminary structural analysis of recombinant bryodin 1, a ribosome-inactivating protein from the plant *Bryonia dioica*, Biochemistry 36 (1997) 3095–3103.
[10] X. Hou, E.J. Meehan, J. Xie, M. Huang, M. Chen, L. Chen, Atomic resolution structure of cucurmosin, a novel type 1 ribosome-inactivating protein from the sarcocarp of Cucurbita moschata, J. Struct. Biol. 164 (2008) 81–87.
[11] Y.R. Yuan, Y.N. He, J.P. Xiong, Z.X. Xia, Three-dimensional structure of beta-momorcharin at 2.55 resolution, Acta Crystallogr. D: Biol. Crystallogr. 55 (1999) 1144–1151.
[12] G.S. Kushwaha, S. Yamini, M. Kumar, M. Sinha, P. Kaur, S. Sharma, T.P. Singh, First structural evidence of sequestration of mRNA cap structures by type 1 ribosome inactivating protein from *Momordica balsamina*, Proteins 81 (2012) (2013) 896–905.
[13] G.S. Kushwaha, N. Pandey, M. Sinha, S.B. Singh, P. Kaur, S. Sharma, T.P. Singh, Crystal structures of a type-1 ribosome inactivating protein from *Momordica balsamina* in the bound and unbound states, Biochim. Biophys. Acta 1824 (2012) 679–691.
[14] H.G. Li, P.L. Huang, D. Zhang, Y. Sun, H.C. Chen, J. Zhang, X.P. Kong, S. Lee-Huang, A new activity of anti-HIV and anti-tumor protein GAP31: DNA adenosine glycosidase—structural and modeling insight into its functions, Biochem. Biophys. Res. Commun. 391 (2010) 340–345.
[15] Q. Huang, S. Liu, Y. Tang, S. Jin, Y. Wang, Studies on crystal structures, active-centre geometry and depurinating mechanism of two ribosome-inactivating proteins, Biochem. J. 309 (1995) 285–298.
[16] Z. Otwinowski, W. Minor, Processing of X-ray diffraction data collected in oscillation mode, Methods Enzymol. 276 (1997) 307–326.
[17] A. Vagin, A. Teplyakov, Molecular replacement with MOLREP, Acta Crystallogr. D Biol. Crystallogr. 66 (2010) 22–25.
[18] G.N. Murshudov, A.A. Vagin, E.J. Dodson, Refinement of macromolecular structures by the maximum-likelihood method, Acta Crystallogr. D: Biol. Crystallogr. 53 (1997) 240–255.
[19] Collaborative Computational Project, The CCP4 suite: programs for protein crystallography, Acta Crystallogr. D Biol. Crystallogr. 50 (1994) 760–763.
[20] E. Potterton, P. Briggs, M. Turkenburg, E. Dodson, A graphical user interface to the CCP4 program suite, Acta Crystallogr. D Biol. Crystallogr. 59 (2003) 1131–1137.
[21] T.A. Jones, J.Y. Zou, S.W. Cowan, M. Kjeldgaard, Improved methods for building protein models in electron density maps and the location of errors in these models, Acta Crystallogr. A47 (1991) 110–119.
[22] P. Emsley, K. Cowtan, Coot: model-building tools for molecular graphics, Acta Crystallogr. D Biol. Crystallogr. 60 (2004) 2126–2132.
[23] I.A. Dubuque, F. Luceri, M. Guglielmi, L. Lodovici, L. Giannini, L. Messerini, P. Dolara, M.B. Charland, SigmaPlot for Scientists, Wm. C. Brown Communications, Inc., 1995.
[24] G. Scatchard, The attractions of proteins for small molecules andions, Ann. N.Y. Acad. Sci. 51 (1949) 660–673.
[25] G.N. Ramachandran, V. Sasisekharan, Conformation of polypeptides and proteins, Adv. Protein Chem. 23 (1968) 283–438.
[26] R.A. Laskowski, M.W. MacArthur, D.S. Moss, J.M. Thornton, PROCHECK: a program to check the stereochemical quality of protein structures, J. Appl. Crystallogr. 26 (1993) 283–291.